Control Engineering Practice 81 (2018) 114–128

Contents lists available at ScienceDirect

Control Engineering Practice

journal homepage: www.elsevier.com/locate/conengprac

Lithium-ion battery state of charge estimation with model parameters adaptation using H_∞ extended Kalman filter

Linhui Zhao [a,*], Zhiyuan Liu [a], Guohuang Ji [b]

[a] Department of Control Science and Engineering, Harbin Institute of Technology, Harbin 150001, China
[b] China FAW Group Corporation New Energy Vehicle Branch, Changchun 130122, China

ARTICLE INFO

Keywords:
Electric vehicle
Lithium-ion battery
State of charge
Model uncertainties
H_∞ extended Kalman filter
Model parameters adaptation

ABSTRACT

Model-based methods can effectively improve the estimation accuracy of state of charge (SOC) for lithium-ion batteries in electric vehicles. Due to the influence of complex electrochemical mechanism and other factors such as temperature, model uncertainties, including unmodeled dynamics and varying parameters, result in that it is difficult to obtain accurate estimation of the SOC using an equivalent circuit model with fixed parameter values under various working conditions of battery. In this paper, two nonlinear models based on single and dual RC models are established, and observability of the nonlinear models is discussed. To bound the influence of model uncertainties, an H_∞ extended Kalman filter is proposed based on robust control theory to estimate the SOC, Ohmic and polarization resistances simultaneously. The performance and robustness of the proposed method are evaluated and compared with a standard extended Kalman filter using multi-temperature datasets. The experimental results show that the proposed method is capable to estimate the SOC more accurately over a large operating range of battery. Furthermore, the validation results of datasets from a battery management system confirm that the proposed method can achieve good performance for real life conditions in a battery pack of electric vehicles.

1. Introduction

Rechargeable batteries are electrochemical systems for storing energy in the form of chemical reactants (Tie & Tan, 2013). Among highly practical and effective technologies for electrochemical energy storage systems, lithium-ion batteries have a wide range of applications as power sources for electric vehicles (EVs) due to its relatively high energy density and long service life (Jaguemont, Boulon, & Dubé, 2016) and are considered in this paper. An effective battery management system (BMS) should evaluate the remaining amount of energy stored in the battery, power capability, and health for a reliable operation and optimal performance of battery powered EVs. These all need to achieve a reliable state of charge (SOC) for the battery (Lu, Han, Li, Hua, & Ouyang, 2013; Zhao, Ji, & Liu, 2017). However, the SOC cannot be measured directly due to the complex electrochemical processes that occur during power transfer to/from the battery. This demands that the SOC has to be estimated online by using the available measurements of the BMS, such as temperature, current, and terminal voltage of the battery.

A necessity for a viable method to estimate the SOC resulted in a broad discussion in the literature as shown in Du, Liu, and Wang (2014) and Wang, Cao, Chen, and Wang (2007). A straightforward method for the SOC estimation is Coulomb counting (Ng, Moo, Chen, & Hsieh, 2009), which depends on the initial value of the SOC and charging/discharging current of the battery. Therefore, the initial SOC error and the accumulated error in the integration process have a direct effect on the SOC estimation.

To improve the accuracy of the SOC estimation, many different model-based methods have been presented in recent years, such as Luenberger observer (Barillas, Li, Günther, & Danzer, 2015; Hu, Sun, & Zou, 2010), sliding mode observer (Chen, Shen, Cao, & Kapoor, 2014; Kim, 2006), and nonlinear observer (Zhao et al., 2017). In addition, Kalman filter (KF) is employed to estimate the SOC (Mastali et al., 2013), and extended Kalman filter (EKF) is used for nonlinear equivalent circuit models to improve the accuracy of the SOC estimation further (Plett, 2004). In this reference, EKF is used to estimate the SOC based on a zero-state hysteresis battery model, in which no RC branch has been considered. EKF is fairly well proven for the SOC estimation problem, even though its theoretical properties like convergence are non-trivial. Moreover, EKF is a standard plug-and-play method that does not require complicated nonlinear theoretical analysis for its design. Additionally, an adaptive extended Kalman filter (AEKF), which employs a covariance matching approach, is used in He, Rui, and Guo (2012), Xiong, Sun, Gong, and He (2013), and Zhang, Cheng, Lu, and Gu (2017) to enhance the performance of EKF for the SOC estimation. Similarly, Sun, Hu, Zou,

* Corresponding author.
E-mail address: zhaolinhui@hit.edu.cn (L. Zhao).

https://doi.org/10.1016/j.conengprac.2018.09.010
Received 12 January 2018; Received in revised form 25 June 2018; Accepted 9 September 2018
Available online 21 September 2018

and Li (2011) presents an adaptive unscented Kalman filter (AUKF) for the SOC estimation based on a zero-state hysteresis battery model.

To improve the robust performance of the SOC estimation, Lin, Mu, Xiong, and Shen (2016), Yan, Xu, Qian, and Xu (2010), and Zhang, Liu, Fang, and Wang (2012) propose a linear matrix inequality (LMI) based H_∞ filter to estimate the SOC. The filter gains are determined by solving a LMI optimization problem in offline mode. In Chen, Xiong, and Shen (2018), dual H_∞ filters are presented to estimate the SOC and capacity of battery. (Yu, Xiong, Lin, Shen, & Deng, 2017) employs an H_∞ filter for model parameters estimation and an UKF for the SOC estimation.

The model-based methods can enhance the robustness and accuracy of the SOC estimation. Equivalent circuit models (ECMs) and electrochemical models are commonly used to estimate the SOC (Zhao et al., 2017). This paper forces on the ECM-based methods due to the ECM is simple and well-suited for observer design. However, a battery model with fixed parameter values is difficult to describe the dynamic process of the battery accurately under different conditions due to the influence of temperature, SOC, charging/discharging current, and other factors (He, Liu, Zhang, & Chen, 2013; Hu & Jung, 2013; Norian, 2013; Waag, Käbitz, & Sauer, 2013), especially for the ECMs with fixed parameters. This makes that the published estimation methods based on a fixed-parameter EMC are difficult to be valid over a large operating range of the battery. As an alternative approach that faces this problem, the electrochemical models can be utilized to estimate the SOC (Dey, Ayalew, & Pisu, 2015; Han, Ouyang, Lu, & Li, 2015; Hu, Cao, & Egardt, 2018) because the electrochemical models can possess physical insight and compensate the influence of temperature and other factors to a certain extent. However, this topic is out of the scope of this paper.

To overcome the above-mentioned limitation, one solution is to build up a relationship between model parameters and influence factors (such as temperature, SOC, and current) based on experimental data of different conditions in offline mode. It may be in form of tables (Fridholm, Wik, & Nilsson, 2016) or mathematical expressions (Sepasi, Ghorbani, & Liaw, 2014). It can accurately provide values of model parameters for different conditions if sufficient complete experimental datasets of the battery are available. Since the working conditions of the batteries in EVs are very complicated, it is not an easy thing to obtain complete experimental datasets. In addition, this method requires a good consistency of the cells in the battery pack. The other is to obtain the values of battery model parameters online by estimating or identifying (Khan, Mulder, & Mierlo, 2014). Since the Ohmic resistance is the main reason for the internal temperature rise of the battery and can quantitatively indicate the battery's aging level, it also provides useful information for determining the battery's internal temperature and state of health by a real-time estimation of the battery resistance (Debert, Colin, Bloch, & Chamaillard, 2013; Du, Liu, Wang, & Wen, 2016).

Among the existing methods for estimating the SOC with model parameters adaptation, Chaoui and Gualous (2017) and Chiang, Sean, and Ke (2011) achieve the simultaneous estimation of open circuit voltage (OCV) and internal resistance of the battery by using adaptive control approach of linear system. Feng, Lu, Wei, and Zhu (2015), He et al. (2012), and Xiong, He, Sun, and Zhao (2013) propose methods for estimating the OCV and model parameters based on an AEKF. Then, the SOC is obtained by looking up table of the OCV versus SOC. For implementing the above-mentioned methods, the SOC–OCV table should have a sufficient accuracy. Additionally, Rahimi-Eichi, Baronti, and Chow (2014) combines least-square parameter identification and Luenberger observer for the SOC estimation. Maral and Liu (2012) uses one UKF for model parameters estimation and the other UKF for the SOC estimation. Similarly, He, Xiong, Zhang, Sun, and Fan (2011) employees an EKF for model parameters estimation and an AEKF for the SOC estimation. It is noted that the above-mentioned methods employ a dual-observer structure to achieve the SOC estimation.

As follows from the above discussion, the battery model uncertainties, including unmodeled dynamics and varying parameters, may deteriorate the SOC estimation significantly. In this paper, an H_∞ EKF (HEKF) is proposed to estimate the SOC and model parameters simultaneously, which can guarantee an upper bound of the estimation errors. Different from the existing methods, the proposed method only uses one estimator to achieve the SOC and model parameters estimation. Furthermore, it can balance the tradeoff between H_∞ and minimum variance performances of EKF.

The main contribution of the paper is that an HEKF is proposed for online estimation of the SOC and model parameters based on robust control theory. Firstly, a random walk is chosen to model Ohmic and polarization resistances of single and dual RC models, respectively. Secondly, the observability of the nonlinear models is discussed using Lie derivative, and the HEKF without solving LMI problems online is proposed. More importantly, the results of performance and robustness tests show that the proposed method is more efficiently in comparison with a standard EKF and is valid over a large operating range of battery voltage, current, SOC, and temperature. In addition, the proposed method based on the single RC model can also achieve good performance with less computational time. This is important for the implementation of the estimation algorithm because of the limitation of computing resources of embedded hardware.

The remainder of this paper proceeds as follows. Section 2 presents single and dual RC models. The proposed method is revealed in Section 3. Section 4 contains the measurement equipment and validation tests, identification of the coefficients of SOC–OCV function, selection of the initial states and polarization capacitances, detailed validation and discussion of the proposed method. The proposed method is further validated based on datasets from a BMS in an EV's battery pack in Section 5. In consequence, Section 6 concludes the research with suggestions for future studies.

2. Lithium-ion battery model

The SOC is defined as the percentage of the releasable capacity relative to the battery rated capacity and is described by Zhao et al. (2017):

$$Soc(t) = Soc(t_0) - \frac{1}{C_N}\int_{t_0}^{t} \eta i_L(t)dt, \tag{1}$$

where $Soc(t_0)$ and $Soc(t)$ are the initial and current SOC of the battery, C_N denotes the battery rated capacity, i_L is the current through the battery ($i_L > 0$ for discharge and $i_L < 0$ for charge), η is the Coulombic efficiency, which is taken as 1 in this paper.

As discussed above, the equivalent circuit models are considered in this paper. Fig. 1 shows two commonly used equivalent circuit models, a single RC model and a dual RC model. As seen in Fig. 1, U_{oc} and U_L are the battery's OCV and terminal voltage, and an Ohmic resistance R_0 is used to characterize the battery's charging or discharging energy losses. R_{pa}, R_{pc}, C_{pa} and C_{pc} character the polarization resistances and capacitances respectively. In the models, the self-discharge resistance is not considered as the lithium-ion batteries have extremely low self-discharge current at load conditions. U_{pa} and U_{pc} are the terminal voltage of the polarization capacitances.

As validated in Hu, Li, and Peng (2012), the single and dual RC models can achieve good performance. To provide different choices for different applications, both models are used to estimate the SOC in this paper, and the estimation accuracy and computation time of the proposed method based on different models are compared and discussed in Sections 4 and 5.

Based on Kirchhoff's voltage law and the models in Fig. 1, the terminal voltage U_L can be calculated using the OCV, the polarization voltages, the current measurement, and the Ohmic resistance of the battery. For the dual RC model, their relationship can be described as (Zhao et al., 2017):

$$U_L(t) = U_{oc}(t) - U_{pa}(t) - U_{pc}(t) - i_L(t)R_0. \tag{2}$$

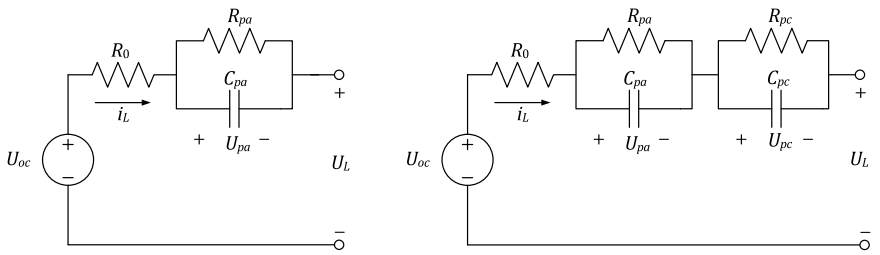

(a) Single RC model. (b) Dual RC model.

Fig. 1. Schematic of equivalent circuit models.

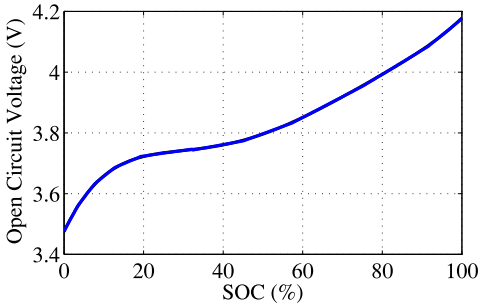

Fig. 2. Measured SOC–OCV curve of a lithium-ion battery cell.

For the single RC model, it is:

$$U_L(t) = U_{oc}(t) - U_{pa}(t) - i_L(t)R_0. \tag{3}$$

As seen in Fig. 2, the relationship between U_{oc} and the SOC is obviously nonlinear. In this paper, it is described by a polynomial function as:

$$U_{oc}(t) = \sum_{i=0}^{m} k_i Soc(t)^i, \tag{4}$$

with coefficients k_i, $i = 0, \ldots, m$. By fitting experimental data of OCV using different order polynomials, m is taken as 6 to achieve enough accuracy. The SOC–OCV function given by Eq. (4) will be validated in Section 4.2.

According to Fig. 1, the dynamics of the voltages across the polarization capacitances can be described as follows:

$$\begin{aligned} \dot{U}_{pa}(t) &= -U_{pa}(t)/\left(R_{pa}C_{pa}\right) + i_L(t)/C_{pa}, \\ \dot{U}_{pc}(t) &= -U_{pc}(t)/\left(R_{pc}C_{pc}\right) + i_L(t)/C_{pc}, \end{aligned} \tag{5}$$

and the dynamics of the SOC according to Eq. (1) is:

$$\dot{S}oc(t) = -\eta i_L(t)/C_N. \tag{6}$$

3. SOC estimation algorithm

3.1. Estimation model

The aim of this paper is to achieve a robust estimation of the SOC for the lithium-ion battery cell of EVs based on the single and dual models shown in Fig. 1. As discussed above, all model parameters have relationships with temperature, SOC, and charging/discharging current of the battery. The effects of different parameters on the cell output (terminal voltage) are evaluated by using statistical multi-parametric sensitivity analysis (MPSA) (Zhao, Gao, Massonnat, Dou, & Miraoui, 2015). The analysis results show that the Ohmic and polarization resistances have higher impact on the battery terminal voltage than the polarization capacitances. Thus, the Ohmic and polarization resistances will be estimated together with the SOC to compensate the effects of model parameter uncertainties.

The relationships between the Ohmic and polarization resistances, temperature, SOC, and charging/discharging current of battery are difficult to be accurately described by mathematical expressions. A random walk is widely used in physics, economics and mathematics, and its definition can be given as a stochastic process that consists of a sequence of changes each of whose magnitude or direction is determined by chance (Doğanaksoy, Çalık, Sulak, & Turan, 2006). A commonly used random walk model is as follows:

$$x(t_k) = x(t_{k-1}) + e(t_k), \tag{7}$$

where $x(t_k)$ is time series, and $e(t_k)$ is random term. So in this paper, a random walk is chosen to model the Ohmic and polarization resistances.

For the dual RC model, define $\boldsymbol{x} = [U_{pa}\ U_{pc}\ Soc\ R_0\ 1/R_{pa}\ 1/R_{pc}]^T$ as the system state vector, the system input $u = i_L$, and the output $y = U_L$. By combining Eqs. (2)~(6) and taking process and measurement noises into count, the battery dynamics can be represented as:

$$\begin{aligned} \dot{\boldsymbol{x}}(t) &= \boldsymbol{f}\left(\boldsymbol{x}(t), u(t)\right) + \boldsymbol{w}(t), \\ y(t) &= h\left(\boldsymbol{x}(t), u(t)\right) + v(t), \end{aligned} \tag{8}$$

with

$$\boldsymbol{f}\left(\boldsymbol{x}(t), u(t)\right) = \begin{bmatrix} -x_1x_5/C_{pa} + u/C_{pa} \\ -x_2x_6/C_{pc} + u/C_{pc} \\ -\eta u/C_N \\ 0 \\ 0 \\ 0 \end{bmatrix}, \quad \boldsymbol{w}(t) = \begin{bmatrix} w_1 \\ w_2 \\ w_3 \\ w_4 \\ w_5 \\ w_6 \end{bmatrix},$$

$$h\left(\boldsymbol{x}(t), u(t)\right) = \sum_{i=0}^{6} k_i x_3^i - x_1 - x_2 - ux_4,$$

and $\boldsymbol{w}(t)$ denotes the augmented process noise that is composed of the process noise and white noise of each model parameter to be estimated, and $v(t)$ is the measurement noise. The augmented process noise and measurement noise are provided to satisfy the following conditions:

$$\begin{aligned} &E[\boldsymbol{w}(t)] = 0, \\ &E[v(t)] = 0, \\ &E[\boldsymbol{w}(t)\boldsymbol{w}^T(\tau)] = \boldsymbol{Q}(t)\delta(t-\tau), \\ &E[v(t)v^T(\tau)] = \boldsymbol{R}(t)\delta(t-\tau), \\ &E[\boldsymbol{w}(t)v^T(\tau)] = 0, \end{aligned} \tag{9}$$

where $\boldsymbol{Q}(t)$ is the system process noise covariance matrix, $\boldsymbol{R}(t)$ is the corresponding measurement noise covariance matrix, and $\delta(t-\tau)$ is the Kronecker delta function, that is $\delta(t-\tau) = 1$ if $t = \tau$, and $\delta(t-\tau) = 0$ if $t \neq \tau$.

Similarly, define the system state vector as $\boldsymbol{x} = [U_{pa}\ Soc\ R_0\ 1/R_{pa}]^T$, the battery dynamics for the single RC model can be written as:

$$\begin{aligned} \dot{\boldsymbol{x}}(t) &= \boldsymbol{f}\left(\boldsymbol{x}(t), u(t)\right) + \boldsymbol{w}(t), \\ y(t) &= h\left(\boldsymbol{x}(t), u(t)\right) + v(t), \end{aligned} \tag{10}$$

with

$$\boldsymbol{f}\left(\boldsymbol{x}(t), u(t)\right) = \begin{bmatrix} -x_1x_4/C_{pa} + u/C_{pa} \\ -\eta u/C_N \\ 0 \\ 0 \end{bmatrix}, \quad \boldsymbol{w}(t) = \begin{bmatrix} w_1 \\ w_2 \\ w_3 \\ w_4 \end{bmatrix},$$

$$h\big(\boldsymbol{x}(t),u(t)\big)=\sum_{i=0}^{6}k_i x_2^i-x_1-ux_3.$$

3.2. Observability of the model

According to Eqs. (8) and (10), the battery dynamics is nonlinear. For the nonlinear state space formulation, the observability definition is local and uses the Lie derivative (Hermann & Krener, 1977). It is a function of estimated state trajectory and inputs applied to the model.

For the system described by Eq. (10), the observability function is:

$$\boldsymbol{o}\big(\boldsymbol{x}(t),u(t)\big)=\begin{bmatrix} h \\ \sum_{i=1}^{4}\big(\frac{\partial h}{\partial x_i}\cdot f_i\big) \\ \sum_{i=1}^{4}\Big(\frac{\partial\sum_{i=1}^{4}\big(\frac{\partial h}{\partial x_i}\cdot f_i\big)}{\partial x_i}\cdot f_i\Big) \\ \sum_{i=1}^{4}\Big(\frac{\partial\sum_{i=1}^{4}\Big(\frac{\partial\sum_{i=1}^{4}\big(\frac{\partial h}{\partial x_i}\cdot f_i\big)}{\partial x_i}\cdot f_i\Big)}{\partial x_i}\cdot f_i\Big) \end{bmatrix}, \tag{11}$$

where h is used instead of the terms $h\big(\boldsymbol{x}(t),u(t)\big)$ for notational simplicity, and f_i is used instead of the terms $f_i\big(\boldsymbol{x}(t),u(t)\big)$, which is an element of the vector $\boldsymbol{f}\big(\boldsymbol{x}(t),u(t)\big)$ with $i=1,\ldots,4$.

By substituting Eq. (10) into Eq. (11), the observability function is therefore expressed as:

$$\boldsymbol{o}=\begin{bmatrix} \sum_{i=0}^{6}k_i x_2^i-x_1-ux_3 \\ (x_1x_4-u)/C_{pa}-\eta u\big(\sum_{i=1}^{6}ik_i x_2^{i-1}\big)/C_N \\ (u-x_1x_4)x_4/C_{pa}^2+(\eta u)^2\big(\sum_{i=2}^{6}i(i-1)k_i x_2^{i-2}\big)/C_N^2 \\ (x_1x_4-u)x_4^2/C_{pa}^3-(\eta u)^3\big(\sum_{i=3}^{6}i(i-1)(i-2)k_i x_2^{i-3}\big)/C_N^3 \end{bmatrix}. \tag{12}$$

If the observability function $\boldsymbol{o}$ is invertible at the current state and input, the system is observable. This function $\boldsymbol{o}$ is invertible if its Jacobian matrix $\boldsymbol{O}$ has a full rank, and the Jacobian matrix $\boldsymbol{O}$ is defined as:

$$\boldsymbol{O}(\boldsymbol{x},u)=\frac{\partial}{\partial\boldsymbol{x}}\boldsymbol{o}(\boldsymbol{x},u). \tag{13}$$

For the system (10), its Jacobian matrix can be written as:

$$\boldsymbol{O}=\begin{bmatrix} -1 & \sum_{i=1}^{6}ik_i x_2^{i-1} & -u & 0 \\ \frac{x_4}{C_{pa}} & \frac{-\eta u\sum_{i=2}^{6}i(i-1)k_i x_2^{i-2}}{C_N} & 0 & \frac{x_1}{C_{pa}} \\ \frac{-x_4^2}{C_{pa}^2} & \frac{(\eta u)^2\sum_{i=3}^{6}i(i-1)(i-2)k_i x_2^{i-3}}{C_N^2} & 0 & \frac{u-2x_1x_4}{C_{pa}^2} \\ \frac{x_4^3}{C_{pa}^3} & \frac{-24(\eta u)^3(k_4+5k_5x_2+15k_6x_2^2)}{C_N^3} & 0 & \frac{3x_1x_4^2-2ux_4}{C_{pa}^3} \end{bmatrix}. \tag{14}$$

It is clear that the rank of the matrix (14) is 4 when $u\neq 0$. This implies that the system (10) is observable if the charging/discharging current of the battery is not equal to zero, and the SOC of the battery is almost unchanged when the current is zero. Similarly, the system (8) is also observable if the charging/discharging current is not equal to zero.

3.3. HEKF algorithm

Since the nonlinearity plays an important role in the single and dual RC models given by Eqs. (8) and (10), KF is not strictly applicable. EKF attempts to overcome this difficulty by using a linearized approximation that is performed at each sample time, and is more suitable for continuous and discrete state variable estimation (Simon, 2012). But the battery model uncertainties, including unmodeled dynamics and varying parameters, may deteriorate the state estimates of EKF significantly. Therefore, an EKF that guarantees a finite upper bound of the estimation error and simultaneously minimize this upper bound is needed. Following the work in Einicke and White (1999), an HEKF is proposed for estimating the SOC in this paper. For a discrete-time state space representation of the battery model:

$$\begin{aligned} \boldsymbol{x}(t_k)&=\boldsymbol{f}_k\big(\boldsymbol{x}(t_{k-1}),u(t_k)\big)+\boldsymbol{w}(t_k),\\ y(t_k)&=h_k\big(\boldsymbol{x}(t_k),u(t_k)\big)+v(t_k), \end{aligned} \tag{15}$$

the H_∞ performance criterion of EKF is defined as:

$$\begin{aligned} \textstyle\sum_{t_k=0}^{N}\|\boldsymbol{x}(t_k)-\hat{\boldsymbol{x}}(t_k)\|^2_{P(t_k)^{-1}}\leqslant\gamma^2\Big(&\|\boldsymbol{x}(0)-\hat{\boldsymbol{x}}(0)\|^2_{P(0)^{-1}}\\ &+\textstyle\sum_{t_k=0}^{N}\big(\|\boldsymbol{w}(t_k)\|^2_{Q(t_k)^{-1}}+\|\boldsymbol{v}(t_k)\|^2_{R(t_k)^{-1}}\big)\Big), \end{aligned} \tag{16}$$

where $\boldsymbol{x}(t_k)$ and $\hat{\boldsymbol{x}}(t_k)$ are the true state vector and its estimates, $\boldsymbol{x}(0)$ and $\hat{\boldsymbol{x}}(0)$ are the true initial state vector and its estimates, $P(0)$ and $P(t_k)$ are the initial and estimated error covariance matrices, γ is a positive scalar parameter that bounds the system uncertainties. This H_∞ criterion indicates that the estimation error of the filter is bounded if the initial state error, process noise, and measurement noise are bounded.

An HEFK is used to achieve the above-mentioned performance. Similar to the standard EKF, the HEKF algorithm is also a recursion, which consists of a prediction step and an update step. The prediction step of the HEKF involves the propagation of both the states and the error covariance estimation between two sampling instants as follows:

$$\begin{aligned} \hat{\boldsymbol{x}}(t_k^-)&=\boldsymbol{f}_k\big(\hat{\boldsymbol{x}}(t_{k-1}),u(t_k)\big),\\ \boldsymbol{P}(t_k^-)&=\boldsymbol{F}(t_{k-1})\boldsymbol{P}(t_{k-1})\boldsymbol{F}(t_{k-1})^T+\boldsymbol{Q}(t_{k-1}). \end{aligned} \tag{17}$$

As seen from (17), the prediction step of the HEKF is similar with the prediction step of the standard EKF. Then, the update step of the HEKF occurs at each sampling time when a new output measurement is available to improve the estimation accuracy as:

$$\begin{aligned} \boldsymbol{K}(t_k)&=\boldsymbol{P}(t_k^-)\boldsymbol{H}(t_k)^T\big(\boldsymbol{H}(t_k)\boldsymbol{P}(t_k^-)\boldsymbol{H}(t_k)^T+\boldsymbol{R}(t_k)\big)^{-1},\\ \hat{\boldsymbol{x}}(t_k)&=\hat{\boldsymbol{x}}(t_k^-)+\boldsymbol{K}(t_k)\big(y(t_k)-\boldsymbol{H}(t_k)\hat{\boldsymbol{x}}(t_k^-)\big),\\ \boldsymbol{P}(t_k)&=\boldsymbol{P}(t_k^-)-\boldsymbol{P}(t_k^-)\begin{bmatrix}-\boldsymbol{H}(t_k)^T & \boldsymbol{I}\end{bmatrix}\\ &\quad\begin{bmatrix}\boldsymbol{H}(t_k)\boldsymbol{P}(t_k^-)\boldsymbol{H}(t_k)^T-\gamma^2\boldsymbol{I} & -\boldsymbol{H}(t_k)\boldsymbol{P}(t_k^-)\\ -\boldsymbol{P}(t_k^-)\boldsymbol{H}(t_k)^T & \boldsymbol{P}(t_k^-)+\boldsymbol{R}(t_k)\end{bmatrix}^{-1}\\ &\quad\begin{bmatrix}-\boldsymbol{H}(t_k)\\ \boldsymbol{I}\end{bmatrix}\boldsymbol{P}(t_k^-), \end{aligned} \tag{18}$$

where $\hat{\boldsymbol{x}}(t_k^-)$ is the forecast of states, $\boldsymbol{P}(t_k^-)$ presents the prediction of error covariances, $\boldsymbol{K}(t_k)$ is the filter gain, $\boldsymbol{I}$ is the unit matrix, $\boldsymbol{F}(t_{k-1})=\partial\boldsymbol{f}_k(\cdot)/\partial\boldsymbol{x}|_{\hat{\boldsymbol{x}}(t_{k-1})}$ and $\boldsymbol{H}(t_k)=\partial h_k(\cdot)/\partial\boldsymbol{x}|_{\hat{\boldsymbol{x}}(t_k^-)}$ are Jacobian matrices obtained from linearization of the state and measurement equations, respectively. By taking the discrete-time form of the system (10) as an example, the explicit expressions of $\boldsymbol{F}(t_{k-1})$ and $\boldsymbol{H}(t_k)$ are as follows:

$$\begin{aligned} \boldsymbol{F}(t_{k-1})&=\begin{bmatrix}1-\frac{T_s\hat{x}_4(t_{k-1})}{C_{pa}} & 0 & 0 & -\frac{T_s\hat{x}_1(t_{k-1})}{C_{pa}}\\ 0 & 1 & 0 & 0\\ 0 & 0 & 1 & 0\\ 0 & 0 & 0 & 1\end{bmatrix},\\ \boldsymbol{H}(t_k)&=\begin{bmatrix}-1 & \sum_{i=1}^{6}k_i\hat{x}_2^{i-1}(t_k^-) & -u(t_k) & 0\end{bmatrix}, \end{aligned} \tag{19}$$

where T_s denotes the sampling time.

As seen from (18), differing from the standard EKF algorithm process, the HEKF employs γ to update the estimated error covariance matrix $P(t_k)$ to bound the estimation error. The detail scheme of the HEKF for the SOC estimation with model parameters adaptation is illustrated in Fig. 3 according to the above-mentioned two steps.

A minimum value for γ^2 in Eq. (18) can be found by searching over $\gamma\neq 0$ such that $\boldsymbol{P}(t_k)$ is positive definiteness. As discussed in Einicke and White (1999), when γ tends to infinity, the HEKF reduces to a

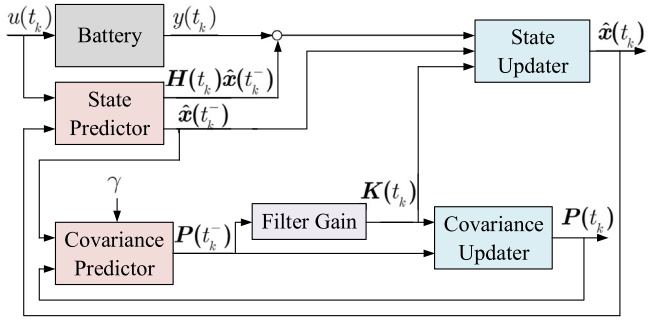

Fig. 3. Block diagram of the HEKF for the SOC estimation.

Table 1
Specifications of the lithium-ion battery cell.

Battery rated capacity	5 Ah
Nominal voltage	3.65 V
Charge limit voltage	4.20 V
Discharge limit voltage	2.75 V
Max. continuous charge current	2.5 A
Max. instant discharge current	7.5 A
Operating temperature range	−20 °C~60 °C

standard EKF. γ can be seen as a tuning parameter to balance the tradeoff between H_∞ performance and minimum variance performance of EKF. Therefore, there is no need to use the minimum possible γ for the SOC and model parameters estimation, and a sample method without solving LMI problems can be used to select the value of γ. Based on Eq. (18), $\boldsymbol{P}(t_k)^{-1}$ can be obtained as:

$$\boldsymbol{P}(t_k)^{-1} = \boldsymbol{P}(t_k^-)^{-1} + \boldsymbol{H}(t_k)^T \boldsymbol{R}(t_k)^{-1} \boldsymbol{H}(t_k) - \gamma^{-2} \boldsymbol{I}. \tag{20}$$

If γ is selected as:

$$\gamma^2 = \varepsilon \max\{eig(\boldsymbol{P}(t_k^-)^{-1} + \boldsymbol{H}(t_k)^T \boldsymbol{R}(t_k)^{-1} \boldsymbol{H}(t_k))^{-1}\}, \tag{21}$$

where ε is a positive constant larger than 1, $\boldsymbol{P}(t_k)^{-1}$ is positive definiteness, and then $\boldsymbol{P}(t_k)$ is positive definiteness.

4. Experimental validation and discussion

The proposed method will be validated and compared with a standard EKF with fixed parameters using experimental datasets of a lithium-ion battery at different temperatures. In this section, the measurement equipment and validation tests, identification of the coefficients of the SOC–OCV function, selection of the initial states and polarization capacitances, detailed validation and discussion of the proposed method will be presented.

4.1. Measurement equipment and validation tests

A battery test bench used in this paper is shown in Fig. 4. It contains four components: (1) An Arbin BT2000 with MITS PRO software (version 4.30) provides a complete control of battery charge and discharge at various modes; (2) A thermal chamber is used to induce a realistic range of ambient temperature during testing; (3) A host computer for online experiment control and data collection; (4) A lithium-ion battery cell under test. The main specifications of the cell under test are presented in Table 1. The sampling time of the battery terminal voltage and current is set as 100 ms.

To achieve sufficient excitations for the cell under test, a test schedule is designed and carried out at different temperatures as prescribed by the United States Advanced Battery Consortium (USABC, 1996) test procedures. The cell is tested at three temperatures (10 °C, 20 °C, and 40 °C) corresponding to a low, normal, and high ambient temperatures during charging and discharging of the cell. In the multi-temperature

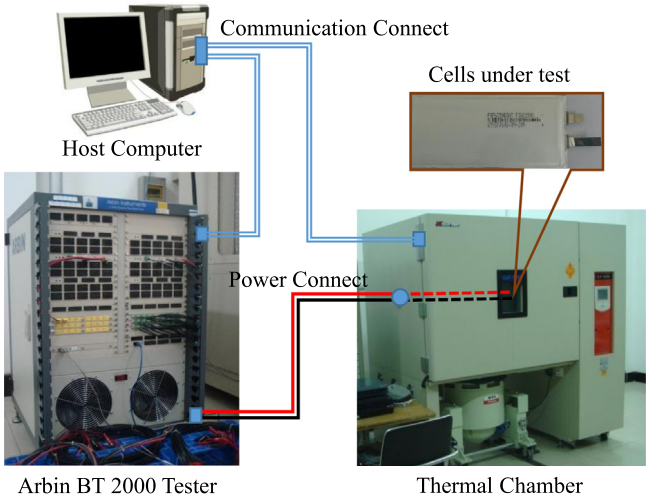

Fig. 4. Schematic diagram of battery test bench.

Table 2
The coefficients of the SOC–OCV function at different temperatures.

Temperatures	k_0	k_1	k_2	k_3	k_4	k_5	k_6
10 °C	3.416	4.074	−20.328	49.800	−61.000	36.910	−8.700
20 °C	3.475	2.786	−11.593	23.078	−20.280	6.713	0
40 °C	3.498	2.108	−8.113	16.034	−13.941	4.579	0

test schedule, a static capacity test, a peak power test, an OCV test, a Dynamic Stress Test (DST), and a Federal Urban Dynamic Schedule (FUDS) are conducted in a consecutive manner. The static capacity test is employed to measure the cell capacity at a designed temperature. The peak power of the cell at different temperatures is obtained through the peak power test and then is used to design the DST and FUDS tests. The datasets of the OCV test will be used to obtain SOC–OCV curves, and then be used to identify the coefficients of the SOC–OCV function. The DST and FUDS tests are used to emulate the actual driving cycles of EVs (Fig. 5). Further detailed description of the multi-temperature test schedule can be found in the authors' previous work (Zhao et al., 2017). In the test schedule, the datasets of the FUDS test will be used to identify the model parameters, and then both DST and FUDS tests will be used to validate the proposed method.

4.2. SOC–OCV coefficients identification

The coefficients of the SOC–OCV function given by Eq. (4) are identified offline by using least-square method based on the datasets of the OCV test at different temperatures. The results are listed in Table 2. To validate the SOC–OCV function, the measured and calculated values of the OCV at different SOCs are shown in Fig. 6. The validation results indicate that the calculated values match the measured values well. Additionally, as seen in Fig. 6, the difference in the initial values of the OCV can be noticed due to the effects of temperature. The robustness of the proposed method to the SOC–OCV coefficient uncertainties will be validated in Section 4.5.

4.3. Initial values of estimated states and polarization capacitances

In general, the initial value of the SOC is stored in the data memory of the BMS, and then is read from the memory when the SOC estimation algorithm starts up. However, there will be an error in the initial SOC if a data loss or a reading data error occurs. This demands that the SOC estimation algorithm should be capable to converge quickly to the correct value of the SOC in this case. To validate the dynamic behavior

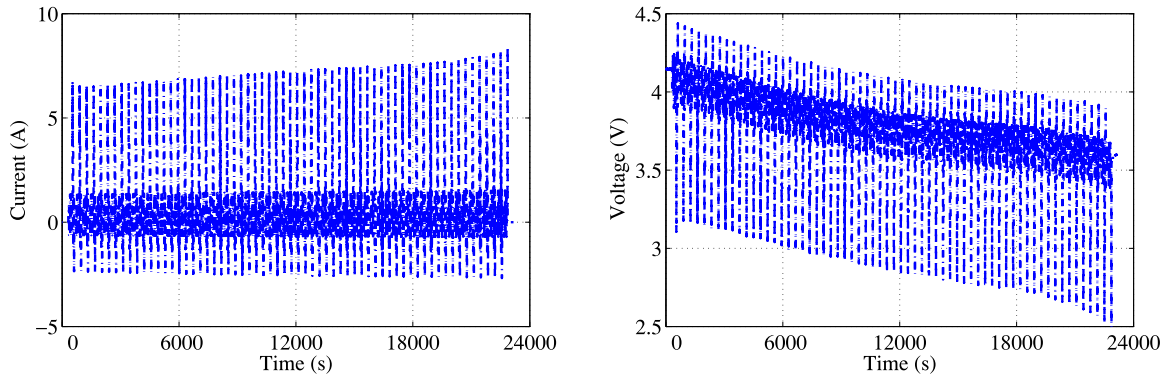

(a) DST.

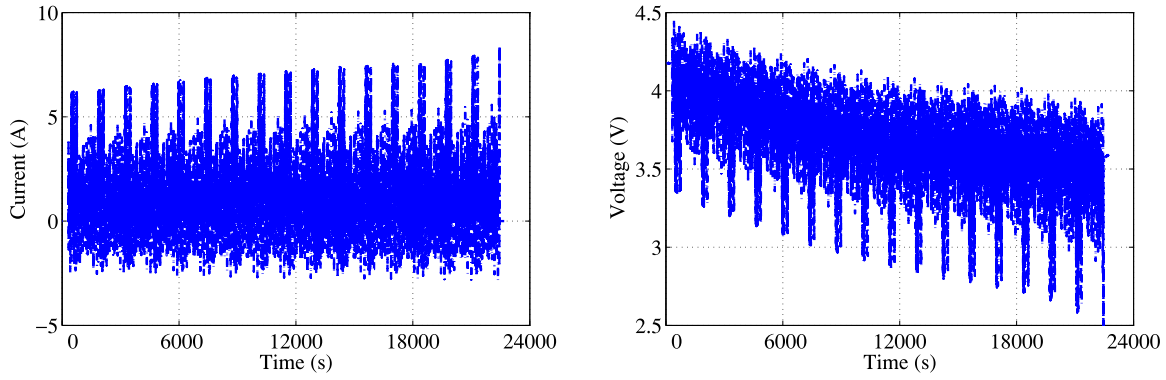

(b) FUDS.

Fig. 5. Dynamic current profiles and voltage responses of the DST and FUDS at 20 °C.

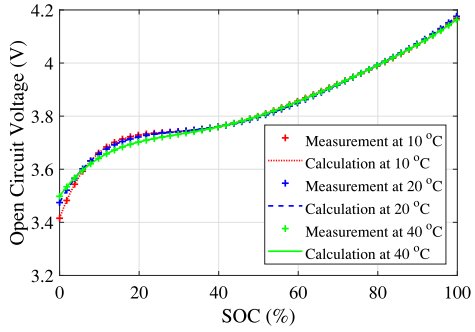

Fig. 6. Validation results of the SOC–OCV function at different temperatures.

of the proposed method, the initial SOC is set as smaller than the actual value of 20% for all datasets.

The initial values of the polarization voltages are set to 0.01 V. The initial Ohmic resistance R_0, polarization resistances R_{pa} and R_{pc} can be chosen as suitable and small values according to the type of battery cell. However, this is not important for the proposed method to obtain an accurate SOC, and the robustness of the proposed method against to different initial values of resistances will be validated and discussed in Section 4.5. In this paper, they are set to 0.1 Ω, 0.01 Ω, and 0.001 Ω, respectively.

In addition, the polarization capacitances C_{pa} and C_{pc} are respectively set to 4000 F and 40000 F. It is worth noting that the initial values of the estimated states and polarization capacitances are the same for the methods based on the single and dual RC models and for all tests in the following.

4.4. Experimental results

The SOC estimation results of the HEKF will be compared with those of a standard EKF with fixed-parameter model as follows:

$$\begin{aligned} \boldsymbol{x}(t_{k+1}) &= \boldsymbol{A}_k \boldsymbol{x}(t_k) + \boldsymbol{B}_k u(t_k) + \boldsymbol{w}(t_k), \\ y(t_k) &= h_k\big(\boldsymbol{x}(t_k), u(t_k)\big) + v(t_k), \end{aligned} \tag{22}$$

with

$$\boldsymbol{A}_k = e^{\boldsymbol{A}T_s},\ \boldsymbol{A} = \begin{bmatrix} -1/\left(R_{pa}C_{pa}\right) & 0 & 0 \\ 0 & -1/\left(R_{pc}C_{pc}\right) & 0 \\ 0 & 0 & 0 \end{bmatrix},$$

$$\boldsymbol{B}_k = \int_0^{Ts} e^{\boldsymbol{A}\tau} d\tau \boldsymbol{B},\ \boldsymbol{B} = \begin{bmatrix} 1/C_{pa} \\ 1/C_{pc} \\ -\eta/C_N \end{bmatrix},$$

$$h_k\big(\boldsymbol{x}(t_k), u(t_k)\big) = \sum_{i=0}^{6} k_i x_3(t_k)^i - x_1(t_k) - x_2(t_k) - R_0 u(t_k).$$

Eq. (22) is a discrete form of the dual RC battery model with fixed parameter values. A modified particle swarm optimization (PSO) algorithm (Mesbahi et al., 2016) is adopted to obtain the values of the model parameters in Eq. (22) in offline mode. As in Wang, Li, Peng, and Liu (2015), by adding differential evolution strategy, the modified PSO algorithm can promote best-performing particles and improve global optimality. Here, a fitness function is defined as:

$$f_{fitness}(\boldsymbol{\theta}) = \sum_{j=1}^{N} \big(y(j) - y(j, \boldsymbol{\theta})\big)^2, \tag{23}$$

with parameter bound

$$\boldsymbol{\theta}_{min} \le \boldsymbol{\theta} \le \boldsymbol{\theta}_{max}, \tag{24}$$

Table 3
Identification results of parameters R_0, R_{pa}, R_{pc}, C_{pa} and C_{pc} at different temperatures.

Temperatures	R_0 (Ω)	R_{pa} (Ω)	R_{pc} (Ω)	C_{pa} (F)	C_{pc} (F)
10 °C	0.126	0.063	0.006	3964	30480
20 °C	0.121	0.052	0.005	4542	52577
40 °C	0.109	0.018	0.002	5865	84719

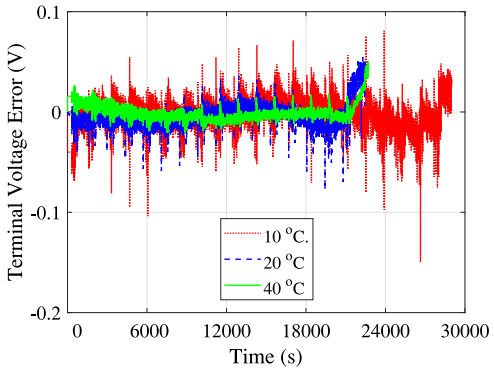

Fig. 7. Validation results of model accuracy at different temperatures.

where $y(j)$ is the measured output which is the battery terminal voltage, $\boldsymbol{\theta} = [R_0\ R_{pa}\ R_{pc}\ C_{pa}\ C_{pc}]^T$ is the model parameter vector, $y(j, \boldsymbol{\theta})$ is the calculated output by using the model (22) and the estimated value of $\boldsymbol{\theta}$, N is the number of test data points, $\boldsymbol{\theta}_{min}$ and $\boldsymbol{\theta}_{max}$ are lower and upper limits of $\boldsymbol{\theta}$. The aim of the MPSO algorithm is to find the value of $\boldsymbol{\theta}$ by minimizing the fitness function $f_{fitness}(\boldsymbol{\theta})$ with constraint (24). The detailed procedure of the modified PSO can be found in Wang et al. (2015).

Using the model (22) and the FUDS datasets at different temperatures, the parameters R_0, R_{pa}, R_{pa}, C_{pa}, and C_{pc} are identified and the results are shown in Table 3. To validate the model (22) and the identification results, the terminal voltage errors, which are the difference between the measured battery terminal voltage and the calculation results based on the model (22) and the parameters shown in Table 3, are shown in Fig. 7. The validation results indicate that the model (22) achieves good fit with experimental data, especially for the experimental data at 20 °C and 40 °C. Additionally, the errors at the end of the tests are obvious due to a low SOC.

For comparing, the SOC measurements, noted as Ref., are determined using the charge capacity and discharge capacity of the battery provided by the test system BT2000, and the results from EKF with fixed model parameter values and the proposed methods are respectively noted as EKF, HEKF-RC, and HEKF-2RC in the following tables and figures.

The choice of the matrices $\boldsymbol{P}$, $\boldsymbol{Q}$, and $\boldsymbol{R}$ is important for the performance and convergence of the EKFs. The initial value of the covariance matrix $\boldsymbol{P}$ (noted as $\boldsymbol{P}_0$) represents mean-squared errors in the knowledge of the initial conditions and affects amplitude of the transient. An ideal choice for the matrices $\boldsymbol{Q}$ and $\boldsymbol{R}$ are the covariance of the corresponding noise. However, any other positive definite matrices can also be chosen as well according to the condition in Reif, Günther, Yaz, and Unbehauen (1999). In this paper, the methodology proposed in Bolognani, Tubiana, and Zigliotto (2003) is used to tune these covariance matrices. The experimental datasets are used to derive appropriate elements of the covariance matrices. For the EKF, by maintaining the element $\boldsymbol{Q}(3,3)$ and $\boldsymbol{R}$, it is found that if there is an initial error of the SOC, the higher $\boldsymbol{Q}(1,1)$ and $\boldsymbol{Q}(2,2)$, the larger estimation error of the SOC in comparison with the effective one because of the lower effect of the battery dynamics. It is worth noting that small values of $\boldsymbol{Q}(1,1)$ and $\boldsymbol{Q}(2,2)$ mean a high reliability of the battery dynamic model. Additionally, it is found that an increment of the element $\boldsymbol{Q}(3,3)$ will result in a faster filter dynamics. But the higher $\boldsymbol{Q}(3,3)$, the larger estimation error of the SOC

Table 4
RMSEs (%) of the estimated SOC for DST and FUDS datasets at different temperatures.

Methods	DST			FUDS		
	10 °C	20 °C	40 °C	10 °C	20 °C	40 °C
EKF	0.56	1.37	0.33	0.60	1.05	0.52
HEKF-RC	0.37	0.38	0.24	0.37	0.70	0.48
HEKF-2RC	0.14	0.36	0.12	0.21	0.51	0.30

if there is a measurement error. Similarly, a large value of $\boldsymbol{R}$ is needed if the measurement of battery terminal voltage has little confidence. However, it will yield a poorer transient response. The tuning procedure provides some guidelines to be followed to set the transient and steady response of the EKFs. It yields the matrices $\boldsymbol{P}_0$, $\boldsymbol{Q}$, and $\boldsymbol{R}$ for the EKF as follows:

$$\begin{aligned} &\boldsymbol{P}_0 = diag(100, 100, 1\times10^5),\\ &\boldsymbol{Q} = diag(10, 10, 1\times10^{-4}),\\ &\boldsymbol{R} = 300. \end{aligned} \tag{25}$$

For the HEKF-2RC, the matrices are chosen as follows:

$$\begin{aligned} &\boldsymbol{P}_0 = diag(10, 10, 3000, 5000, 5000, 5000),\\ &\boldsymbol{Q} = diag(100, 100, 1\times10^{-4}, 5\times10^{-3}, 5\times10^{4}, 5\times10^{4}),\\ &\boldsymbol{R} = 1000. \end{aligned} \tag{26}$$

For the HEKF-RC, $\boldsymbol{P}_0$, $\boldsymbol{Q}$, and $\boldsymbol{R}$ are set as:

$$\begin{aligned} &\boldsymbol{P}_0 = diag(10, 3000, 5000, 5000),\\ &\boldsymbol{Q} = diag(100, 1\times10^{-4}, 5\times10^{-3}, 5\times10^{4}),\\ &\boldsymbol{R} = 1000. \end{aligned} \tag{27}$$

The value of ϵ in Eq. (21) can be selected in a large range and the HEKF always achieves a good performance. 1600 is used in this paper.

In the following, the proposed method will be validated and compared with a standard EKF with fixed model parameter values based on the DST and FUDS datasets at 10 °C, 20 °C and 40 °C, respectively. It is worth noting that a zero-mean-value random noise with Gaussian distribution is added to the measured current and terminal voltage to simulate the most likely cause of the error in the data acquisition process, and the variances are 0.0001 A^2 and 0.0001 V^2, respectively. The estimation results for the DST datasets at different temperatures are plotted in Fig. 8. In addition, those for the FUDS datasets are shown in Fig. 9. In order to compare the estimation accuracy of different methods quantitatively, the root mean square errors (RMSEs) of the estimated SOCs are presented in Table 4.

As seen from Table 4, and Figs. 8 and 9, the proposed method achieves batter accuracy and convergence rate of the SOC estimation for all datasets in comparison with the EKF with fixed model parameter values. Although there is a large initial error (20%) because of the initial SOC setting, the proposed method is capable to achieve an accurate estimation of the SOC in a very short time. Furthermore, the errors of the proposed method are small after the estimation convergence. However, Table 4 shows that the RMSEs of the proposed method based on the dual RC model is slightly smaller than those of the method based on the single RC model, especially for the datasets at 10 °C and 40 °C. One main reason for this is that an extra RC branch in the dual RC model may provide some useful information for the influence of the temperature. In addition, the estimation results of the EKF with fixed model parameter values deteriorate quickly when the SOC is lower than 10%. A main reason is that the values of polarization resistances change with the SOC of the battery significantly in this case.

The above-presented results show that the HEKF can achieve better estimation accuracy than the EKF with fixed parameters. The latter is a common method for the SOC estimation. To further verify the effectiveness of the proposed method, a comparison study of estimation results of the HEKF and an EKF with parameters adaptation has also been carried out based on the datasets at different temperatures. Due to space limitations, the results are not given in the form of figures. Similar with the HEKF, the comparison results show that the EKF with

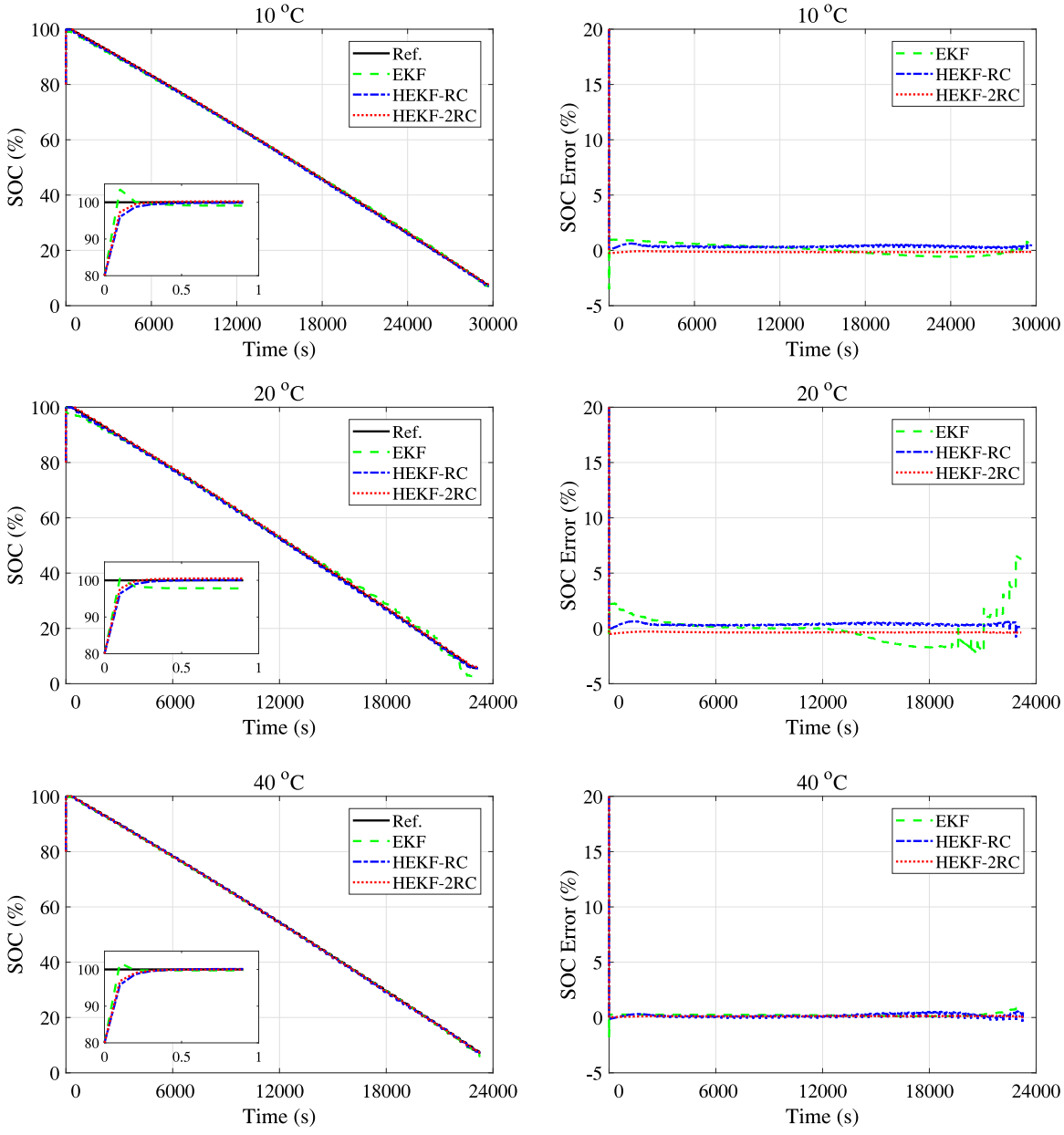

Fig. 8. Estimation results of DST datasets at different temperatures..

parameters adaptation can also achieve good performance. By careful comparison, it is found that the maximum estimation error of the HEKF is smaller than that of the EKF with parameters adaptation. For the DST dataset at 20 °C and the dual RC model, the maximum error of the HEKF and the EKF with parameters adaptation are 0.47% and 1.01% after the estimation convergence. This is mainly because that an H_∞ performance criterion is considered in the HEKF.

Furthermore, to validate the model used in this paper and illustrate the effectiveness of the proposed method, the calculation results of the system output (terminal voltage) based on the model (22) (in open loop mode) are compared with the results in closed loop mode with the HEKF-RC and HEKF-2RC, and their RMSEs for the DST and FUDS datasets at different temperatures are shown in Table 5. Since it is open loop, the calculation results based on model (22) show more errors compared with those from the HEKFs. However, the model shows an acceptable accuracy for all datasets, and the proposed method based on the single and dual RC models can significantly improve the accuracy of the system output.

Table 5
RMSEs (mV) of the system output for DST and FUDS datasets at different temperatures.

Methods	DST			FUDS		
	10 °C	20 °C	40 °C	10 °C	20 °C	40 °C
Model	18.6	18.4	18.1	21.4	18.3	17.2
HEKF-RC	0.82	0.90	0.65	1.85	1.22	0.82
HEKF-2RC	0.82	0.91	0.65	1.84	1.21	0.79

The estimation results of the Ohmic resistance R_0 and polarization resistance R_{pa} for the datasets at different temperatures are shown in Fig. 10. It indicates that the estimated Ohmic resistance based on the DST dataset is almost the same as that based on the FUDS dataset at the same temperature for each model. This is consistent with the actual situation.

By comparing Table 3 and Fig. 10, it is found that the values of the model parameters obtained by offline identification are approximately equal to the average values achieved by online estimation. This is the main reason for improving the accuracy of the SOC estimation with

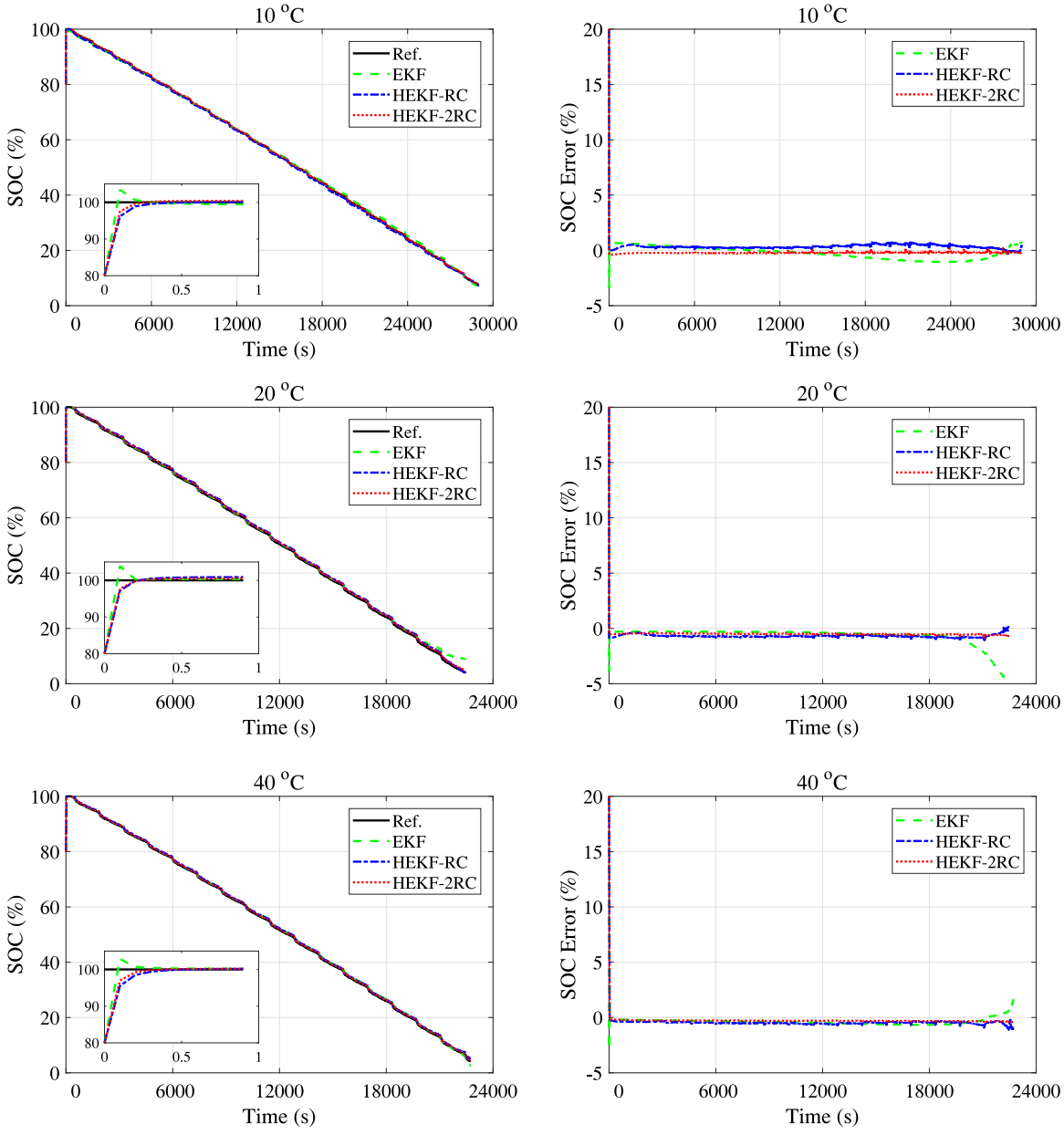

Fig. 9. Estimation results of FUDS datasets at different temperatures..

model parameters adaptation. Moreover, as seen from Fig. 10, the estimated Ohmic resistance changes with temperature obviously, and the SOC has little effect on it. The Ohmic resistance is the main reason for the internal temperature rise of the battery cell during charging and discharging. Therefore, the estimated Ohmic resistance can be used to determine the internal temperature of battery cell, which is difficult to be measured by a sensor. A feasible method is to establish a thermal model to estimate the internal temperature of battery cell by using the estimated Ohmic resistance and measurement of external temperature as shown in Debert et al. (2013).

In addition, as the majority resistance in the equivalent circuit model, the Ohmic resistance can quantitatively indicates the battery's aging level as shown in Prasad and Rahn (2014). The increase of the Ohmic resistance induces the power fade directly, which is an important sign for battery aging. Therefore, the method proposed in this paper can also provide useful information for online determining state of health of the battery by comparing the estimated Ohmic resistances under the same working conditions.

As seen from Fig. 10, the estimated polarization resistance shows more effect by the SOC and the charging/discharging current, especially for the results of datasets at 10 °C and 20 °C. Since the fixed values of polarization capacitances are used in the model, the estimated polarization resistances may couple the uncertainty of polarization capacitances. However, their estimated values can indicate the changing trend of the polarization resistances, and the SOC dependency is in accordance with those in Lin et al. (2013), where the polarization resistances identified at different temperatures are available.

It should be noted that the proposed method based on the dual RC model needs a little more computational time in comparison with the method based on the single RC model. The DST dataset at 10 °C is taken as an example, the average cycle times of the two methods are evaluated in the MATLAB environment. The clock frequency of the used computer is 2.3 GHz. The results are 0.1519 ms and 0.1308 ms, and show that the method based on the single RC mode can save around 14% computational time as compared with the other method. Additionally, Field Programmable Gate Array (FPGA) technology has shown its great potential for the embedded implementation of EKF

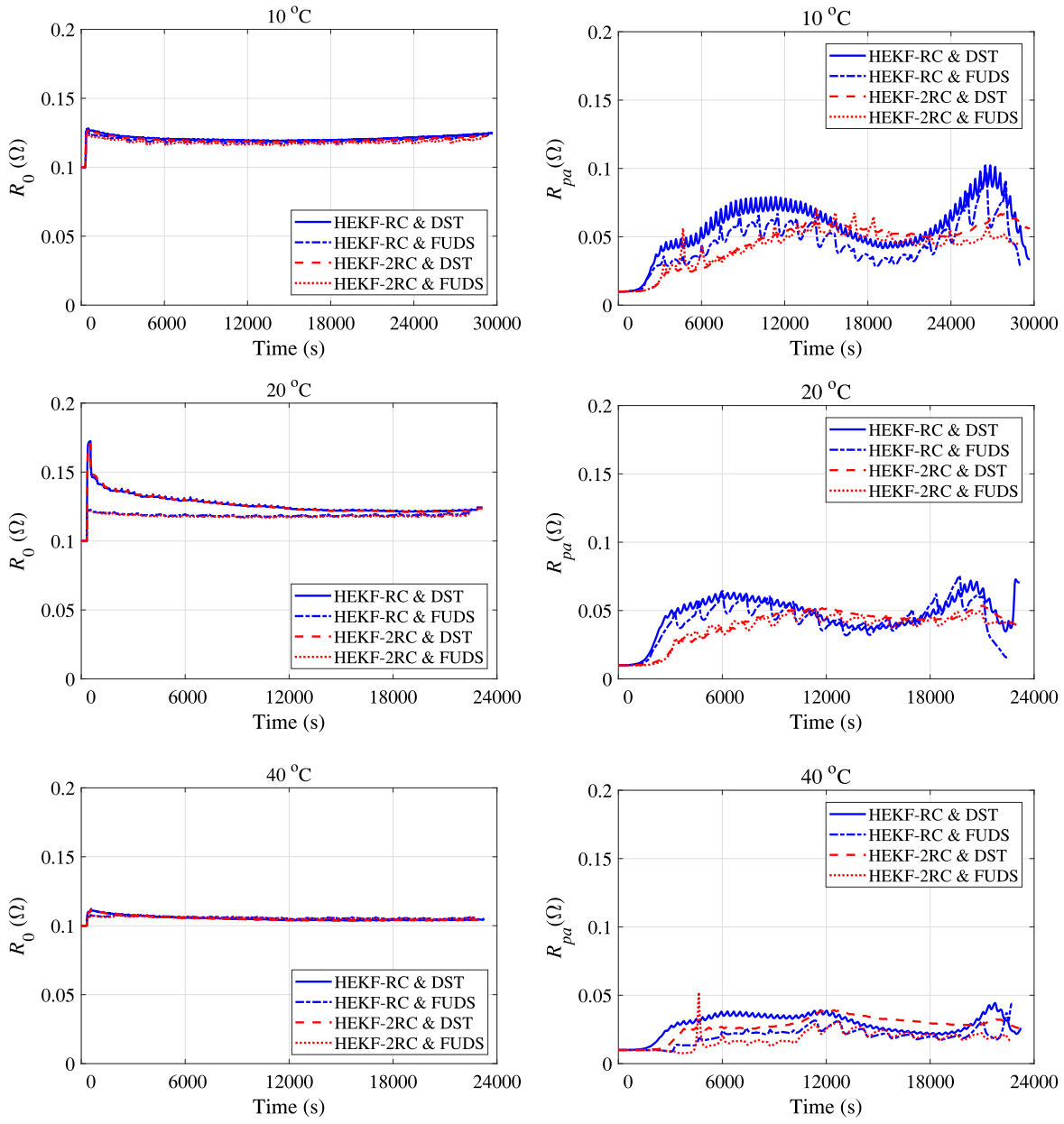

Fig. 10. Estimated Ohmic and polarization resistances at different temperatures..

algorithm (Guo, Chen, Xu, Wang, & Lu, 2013), and can significantly improve the computational efficiency of the estimation algorithm.

4.5. Robustness testing

The above-presented experimental results indicate that the HEKF is capable to obtain a good performance in normal conditions. In the following, the DST dataset at 40 °C will be taken as an example, and the validation results and discussion on robustness testing of different initial values of the estimated resistances, sensor biases, sensor gain change, and model parameter uncertainties for the proposed method will be presented.

The initial values of the Ohmic and polarization resistances are set to only 80% of the initial values used in the above section, and the SOC estimation results presented in Fig. 11 show that the HEKFs are capable of determining the SOC with different initial values of the Ohmic and polarization resistances. This indicates that the initial values of the resistances have little effect on the estimation accuracy of the SOC for the HEKFs.

A current offset may appear caused by an aged current sensor in the BMS. Thus, an offset of 50 mA is introduced into the current measurement to validate the robust performance of the proposed method, and the results are presented in Fig. 12(a). It is worth noting that the maximum current of the DST at 40 °C is about 7.5 A, but its average current is only 0.71 A. The added offset in this test is about 7% of the average current of the DST. As shown in Fig. 12(a), the maximum errors of the estimated SOC of the HEKF-RC and HEKF-2RC are 4.3% and 3.5% respectively. Additionally, the current measurement is multiplied by 1.05 to simulate the change of the current sensor gain, and the results are shown in Fig. 12(b). In this test, the maximum errors of the estimated SOC of the HEKF-RC and HEKF-2RC are 3.4% and 2.8%. It is found that the proposed methods have acceptable robustness against the sensor biases and gain change.

In general, the accurate capacity is difficult to obtain online for an aged cell due to the complex aging mechanism of the battery. Thus, a deviation of 5% is applied to C_N to simulate this case, and the results are shown in Fig. 13(a). The polarization capacitances C_{pa} and C_{pc} are set as a constant value in this paper. To validate the robustness properties of

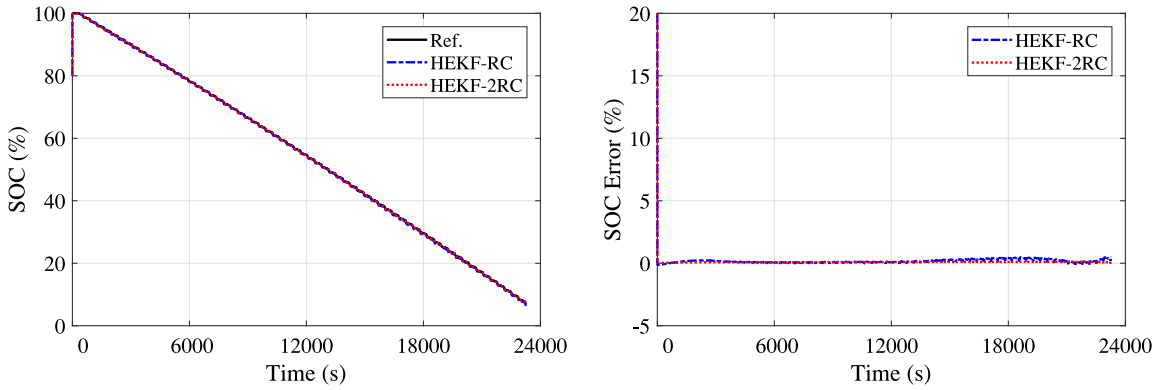

Fig. 11. Robustness testing 1: With different initial values of the estimated resistances.

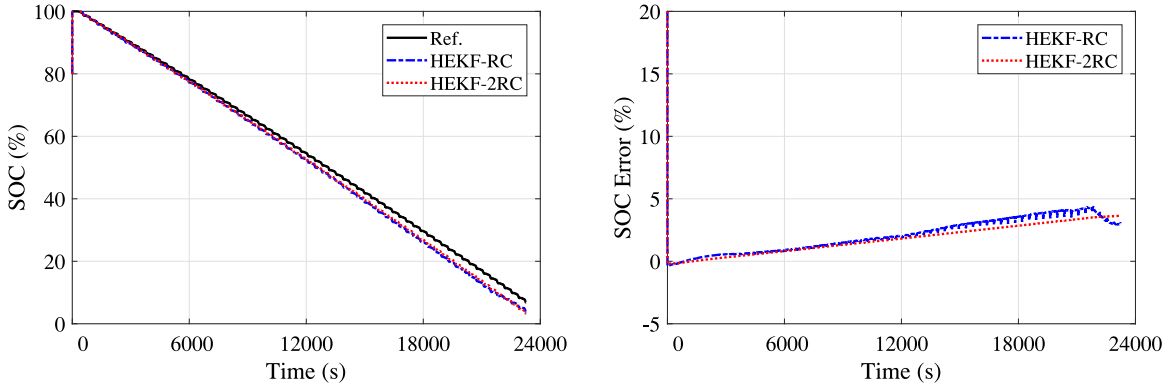

(a) With current sensor biases.

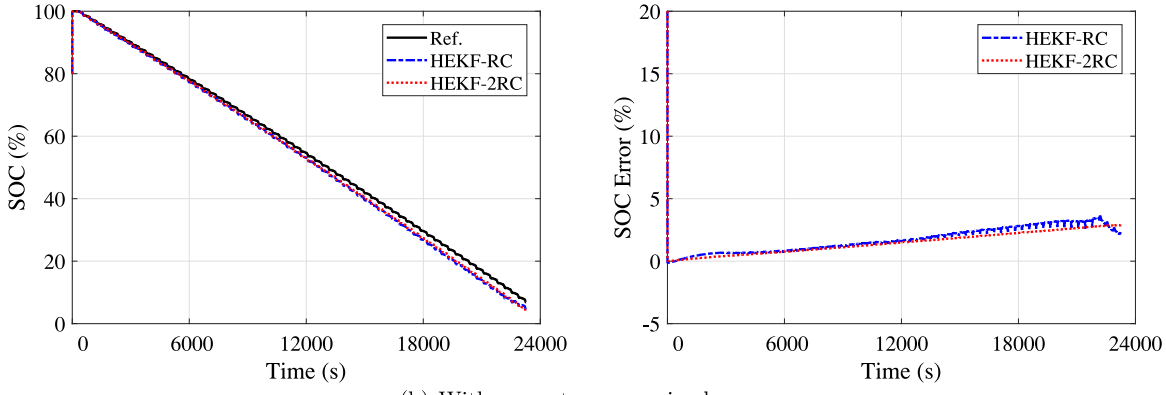

(b) With current sensor gain change.

Fig. 12. Robustness testing 2: With measurement errors.

the two methods with respect to these parameter uncertainties, the C_{pa} and C_{pc} are set to 80% of the values used in the above section, and the SOC estimation results are shown in Fig. 13(b). As shown in Table 2, the temperature has a significant influence on the coefficients of the SOC–OCV function, which is used to approximate the SOC–OCV curve. In the following test, the coefficients obtained from the OCV test dataset at 10 °C are used to the one at 40 °C to simulate the deviation of the SOC–OCV function coefficients due to the influence of temperature, and the estimation results are listed in Fig. 13(c). All the estimation results show that both methods can achieve favorable robustness with respect to different model parameter uncertainties. Moreover, the estimation results shown in Fig. 13(c) indicate that the coefficients of the SOC–OCV function obtained from the OCV test datasets at 10 °C, 20 °C and 40 °C can be used to cover the whole operating temperature range of battery directly. Moreover, if the BMS's storage space is enough to use and OCV test datasets at different temperatures are available, a smaller temperature interval can be selected to improve the calculation accuracy of the OCV, for example 5 °C. To make it convenient for comparing, the RMSEs of the estimated SOC of all the robustness analysis are shown in Table 6.

It worth noting that the effectiveness and applicability of the HEKF can be further improved by estimating the battery capacity C_N together with the SOC and other model parameters. This is considered as our future work.

Due to space limitations, the estimated Ohmic and polarization resistances have not been given here. But the estimation results are very similar with those shown in Fig. 10. This implies that the proposed methods are capable of determining the resistances with different disturbances.

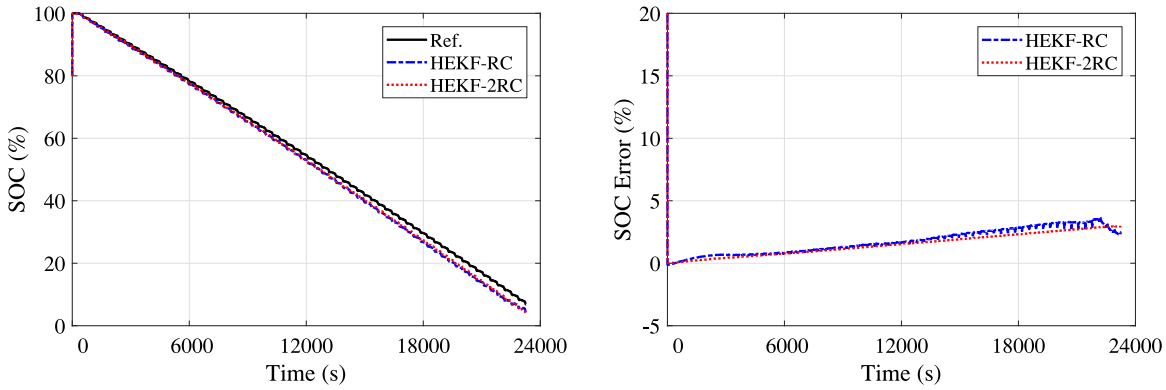

(a) With mode parameter uncertainties caused by capacity deterioration.

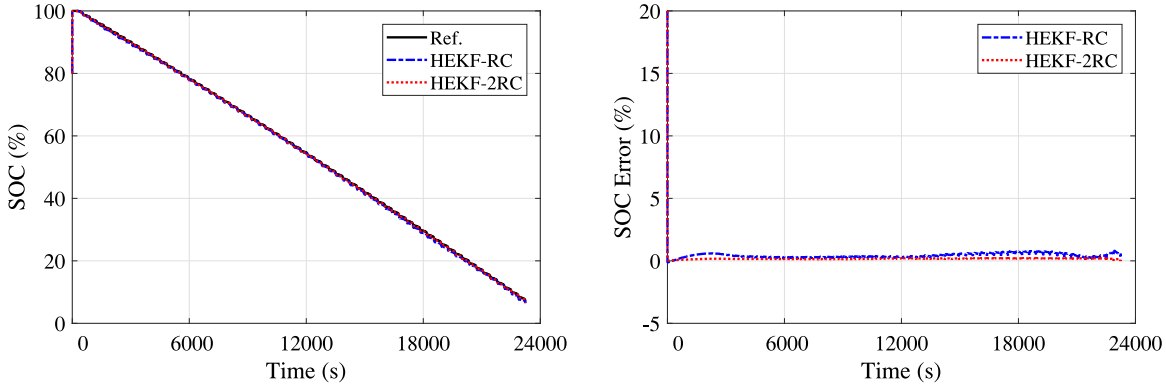

(b) With different polarization capacitances.

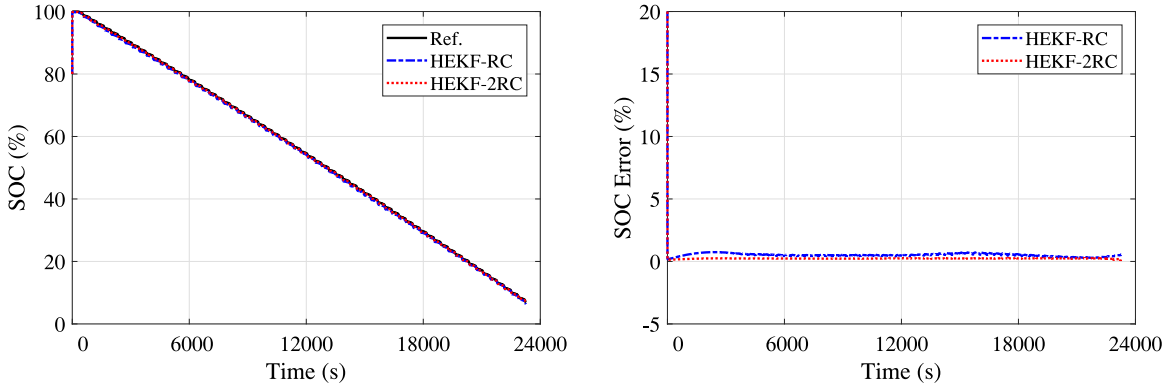

(c) With mode parameter uncertainties caused by coefficients of SOC-OCV function.

Fig. 13. Robustness testing 3: With model parameter uncertainties.

5. Application of HEKF to EV battery

There is a potential application for the HEKF in EVs. Due to different disturbances may appear in real vehicle, this section adopts the New European Driving Cycle (NEDC) test based on an EV battery pack to evaluate the performance of the proposed method. NEDC is a typical driving cycle for EV battery pack. The battery pack is composed of 3200 lithium-ion cells (NCR18650BD from Panasonic) connected in series to achieve the desired voltage and in parallel to meet the capacity requirement.

A real BMS developed by the authors is used to collect voltage and current measurements from sensors mounted on the EV battery pack. Both current and voltage are recorded at a frequency of 10 Hz. The measurements of voltage and current are collected from CAN (Controller Area Network) bus of the BMS by CANoe, which is a tool developed by Vector Informatik GmbH for testing and analysis of automotive control networks. To compare the estimation results, the charge capacity and discharge capacity of battery are measured by the test system BT2000 at the same time and are used to calculate the SOC measurements. The proposed method is validated for different cells in the battery pack based on the datasets collected at different temperatures, and only the measurements and estimation results of one cell at 30 °C are presented in this section because of space limitations.

Differing from the current and terminal voltage are measured by Arbin BT2000 in the above section, Fig. 14(a) shows the dynamic current profile and voltage response of one cell, which are collected by the BMS in the battery pack. For comparing the results in open loop and closed loop modes, the SOC calculation results based on the Eq. (1) and

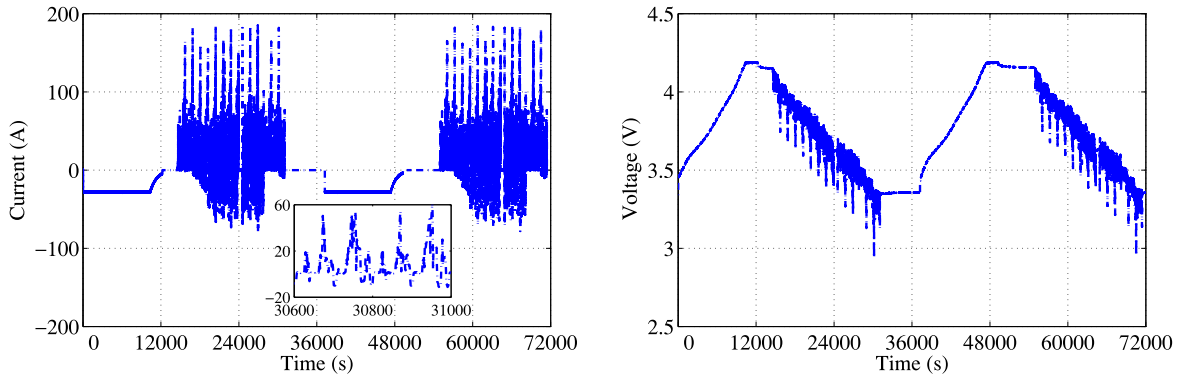

(a) Dynamic current profile and voltage response of NEDC test collected by the BMS.

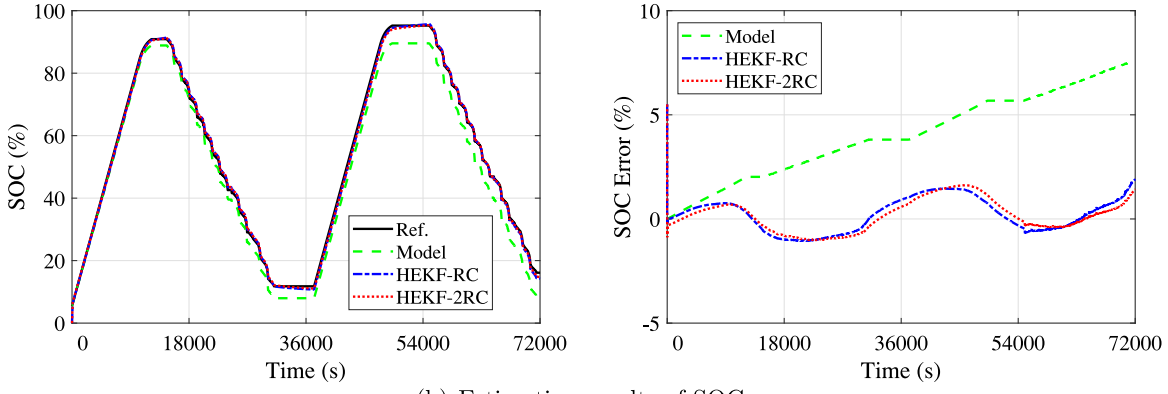

(b) Estimation results of SOC.

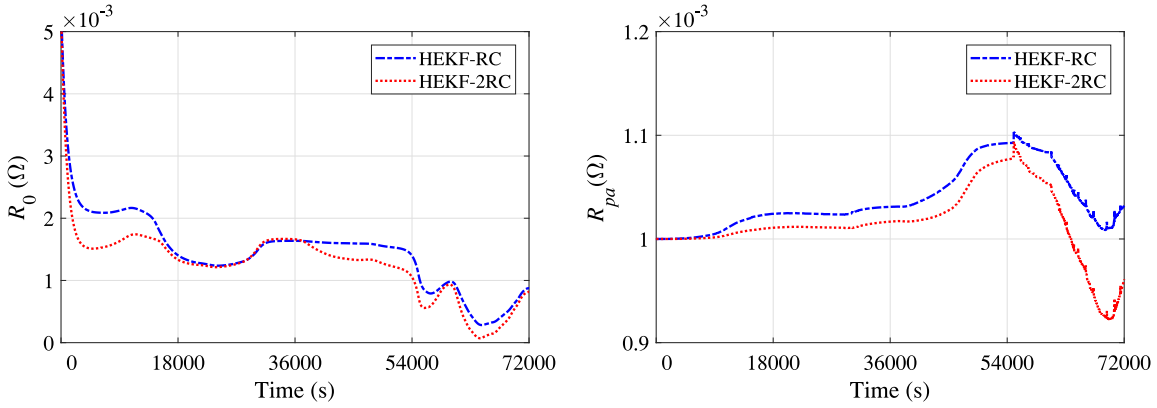

(c) Estimation results of Ohmic and polarization resistances.

Fig. 14. Validation results of datasets from the BMS in an EV battery pack.

the SOC estimation results from the proposed methods are presented in Fig. 14(b). Since the result in open loop is not convergence if there is a initial SOC error, the initial SOC is chosen as its actual value 5.5% in the open mode. Correspondingly, the initial SOC for the proposed methods is set as zero to check the convergence rate. The estimation results of the Ohmic resistance R_0 and polarization resistance R_{pa} are presented in Fig. 14(c).

As seen from Fig. 14, the HEKF based on the single and dual RC models can maintain good performance for such real-life conditions, and the maximum errors of the SOC estimation are no more than 2% after the estimation convergence. As noted in introduction, the open loop method (Coulomb counting) based on Eq. (1) leads to unacceptable results due to the presence of biases and noise in the current measurements of a real vehicle.

Table 6
RMSEs (%) of the estimated SOC all the robustness testing.

Test cases	HEKF-RC	HEKF-2RC
Initial values of resistance	0.47	0.17
Current sensor biases	2.47	2.10
Current sensor gain change	1.98	1.68
Uncertainty of battery capacity	2.02	1.73
Uncertainty of polarization capacitances	0.22	0.10
Uncertainty of SOC–OCV coefficients	0.53	0.24

6. Conclusions

This paper proposes an HEKF based on robust control theory for online estimation of the SOC and model parameters. The proposed

method can guarantee the upper bound of the SOC estimation errors. The SOC estimation results from the proposed method are compared with those from a standard EKF with fixed model parameter values. It demonstrates that the proposed method can achieve relatively good estimation of the SOC for the datasets at different temperatures. The proposed method also shows a favorable robustness and adaptability to different disturbances, such as measurement noise, different initial values of the estimated states, current sensor biases and gain change, and model parameter uncertainties. This confirms that the proposed method can be valid over a large operating range of battery. Since the Ohmic resistance can quantitatively indicate the battery's aging level, and the estimation results show more effect by temperature, the proposed method can provide useful information for determining the battery's internal temperature and state of health. Furthermore, the proposed method is validated based on the datasets from the BMS in an EV battery pack, and achieves good performance for real life conditions. It is worth noting that the proposed method based on the single RC model also shows good performance with less computational time.

Due to the online adaption of model parameters, the influence of complex electrochemical mechanism and other factors such as temperature can be compensated to a certain extent. However, the battery's aging mechanism is very complicated and the battery-aging test requires a long period, our future work will take into account the influence of the battery aging on the model to enhance the performance of the proposed method for aged battery cells. Moreover, the combined estimation of internal temperature and state of health is seen as an area of our future work, since the internal temperature is an important factor that affects the battery cell's ageing and its state of health need to be identified online. It is also under consideration to extend the results of this paper to a battery pack with considering the difference among the cells and the effect of balance control.

Acknowledgments

This work was supported by the China Automobile Industry Innovation and Development Joint Fund, China [grant number U1564213] and the China Scholarship Council, China [No. 201706125075].

References

Barillas, J. K., Li, J., Günther, C., & Danzer, M. A. (2015). A comparative study and validation of state estimation algorithms for Li-ion batteries in battery management systems. *Applied Energy*, *155*, 455–462.

Bolognani, S., Tubiana, L., & Zigliotto, M. (2003). Extended Kalman filter tuning in sensorless PMSM drives. *IEEE Transactions on Industry Applications*, *39*(6), 1741–1747.

Chaoui, H., & Gualous, H. (2017). Online parameter and state estimation of lithium-ion batteries under temperature effects. *Electric Power Systems Research*, *145*, 73–82.

Chen, X., Shen, W., Cao, Z., & Kapoor, A. (2014). A novel approach for state of charge estimation based on adaptive switching gain sliding mode observer in electric vehicles. *Journal of Power Sources*, *246*, 667–678.

Chen, C., Xiong, R., & Shen, W. (2018). A lithium-ion battery-in-the-loop approach to test and validate multiscale dual H infinity filters for state-of-charge and capacity estimation. *IEEE Transactions on Power Electronics*, *33*(1), 332–341.

Chiang, Y. -H., Sean, W. -Y., & Ke, J. -C. (2011). Online estimation of internal resistance and open-circuit voltage of lithium-ion batteries in electric vehicles. *Journal of Power Sources*, *196*, 3921–3932.

Debert, M., Colin, G., Bloch, G., & Chamaillard, Y. (2013). An observer looks at the cell temperature in automotive battery packs. *Control Engineering Practice*, *21*, 1035–1042.

Dey, S., Ayalew, B., & Pisu, P. (2015). Nonlinear robust observers for state-of-charge estimation of lithium-ion cells based on a reduced electrochemical model. *IEEE Transactions on Control Systems Technology*, *23*(5), 1935–1942.

Doğanaksoy, A., Çalık, Ç, Sulak, F., & Turan, M. S. (2006). New randomness tests using random walk. In *Proceedings of national cryptology symposium II*. Ankara, Turkey.

Du, J., Liu, Z., & Wang, Y. (2014). State of charge estimation for li-ion battery based on model from extreme learning machine. *Control Engineering Practice*, *26*, 1–19.

Du, J., Liu, Z., Wang, Y., & Wen, C. (2016). An adaptive sliding mode observer for lithium-ion battery state of charge and state of health estimation in electric vehicles. *Control Engineering Practice*, *54*, 81–90.

Einicke, G. A., & White, L. B. (1999). Robust extended kalman filtering. *IEEE Transactions on Signal Processing*, *47*(9), 2596–2599.

Feng, F., Lu, R., Wei, G., & Zhu, C. (2015). Online estimation of model parameters and state of charge of $LiFePO_4$ batteries using a novel open-circuit voltage at various ambient temperatures. *Energies*, *8*, 2950–2976.

Fridholm, B., Wik, T., & Nilsson, M. (2016). Kalman filter for adaptive learning of look-up tables with application to automotive battery resistance estimation. *Control Engineering Practice*, *48*, 78–86.

Guo, H., Chen, H., Xu, F., Wang, F., & Lu, G. (2013). Implementation of EKF for vehicle velocities estimation on FPGA. *IEEE Transactions on Industrial Electronics*, *60*(9), 3823–3835.

Han, X., Ouyang, M., Lu, L., & Li, J. (2015). Simplification of physics-based electrochemical model for lithium ion battery on electric vehicle. Part II: Pseudo-two-dimensional model simplification and state of charge estimation. *Journal of Power Sources*, *278*, 814–825.

He, Y., Liu, X., Zhang, C., & Chen, Z. (2013). A new model for state-of-charge (SOC) estimation for high-power Li-ion batteries. *Applied Energy*, *101*, 808–814.

He, H., Rui, X., & Guo, H. (2012). Online estimation of model parameters and state-of-charge of $LiFePO_4$ batteries in electric vehicles. *Applied Energy*, *89*, 413–420.

He, H., Xiong, R., Zhang, X., Sun, F., & Fan, J. (2011). State-of-charge estimation of the lithium-ion battery using an adaptive extended Kalman filter based on an improved Thevenin model. *IEEE Transactions on Vehicular Technology*, *60*(4), 1461–1469.

Hermann, R., & Krener, A. (1977). Nonlinear controllability and observability. *IEEE Transactions on Automatic Control*, *22*(5), 728–740.

Hu, X., Cao, D., & Egardt, B. (2018). Condition monitoring in advanced battery management systems: Moving horizon estimation using a reduced electrochemical model. *IEEE/ASME Transactions on Mechatronics*, *23*(1), 167–178.

Hu, T., & Jung, H. (2013). Simple algorithms for determining parameters of circuit models for charging/discharging batteries. *Journal of Power Sources*, *233*, 14–22.

Hu, X., Li, S., & Peng, H. (2012). A comparative study of equivalent circuit models for Li-ion batteries. *Journal of Power Sources*, *198*, 359–367.

Hu, X., Sun, F., & Zou, Y. (2010). Estimation of state of charge of a lithium-ion battery pack for electric vehicles using an adaptive luenberger observer. *Energies*, *3*, 1586–1603.

Jaguemont, J., Boulon, L., & Dubé, Y. (2016). A comprehensive review of lithium-ion batteries used in hybrid and electric vehicles at cold temperatures. *Applied Energy*, *164*, 99–114.

Khan, M. R., Mulder, G., & Mierlo, J. V. (2014). An online framework for state of charge determination of battery systems using combined system identification approach. *Journal of Power Sources*, *246*, 629–641.

Kim, I. -S. (2006). The novel state of charge estimation method for lithium battery using sliding mode observer. *Journal of Power Sources*, *163*, 584–590.

Lin, C., Mu, H., Xiong, R., & Shen, W. (2016). A novel multi-model probability battery state of charge estimation approach for electric vehicles using H_∞ algorithm. *Applied Energy*, *166*, 76–83.

Lin, X., Perez, H. E., Mohan, S., Siegel, J. B., Stefanopoulou, A. G., Ding, Y., et al. (2013). A lumped-parameter electro-thermal model for cylindrical batteries. *Journal of Power Sources*, *232*, 79–85.

Lu, L., Han, X., Li, J., Hua, J., & Ouyang, M. (2013). A review on the key issues for lithium-ion battery management in electric vehicles. *Journal of Power Sources*, *226*, 272–288.

Maral, P., & Liu, G. (2012). Online estimation of model parameters and state-of-charge of lithium-ion battery using unscented Kalman filter. In *Proceedings of the 2012 american control conference* (pp. 3962–3967). Montréal, Canada.

Mastali, M., Vazquez-Arenas, J., Fraser, R., Fowler, M., Afshar, S., & Stevens, M. (2013). Battery state of the charge estimation using kalman filtering. *Journal of Power Sources*, *239*, 294–307.

Mesbahi, T., Khenfri, F., Rizoug, N., Chaaban, K., Bartholomeüs, P., & Moigne, P. L. (2016). Dynamical modeling of Li-ion batteries for electric vehicle applications based on hybrid particle swarm-nelder-mead (PSO-NM) optimization algorithm. *Electric Power Systems Research*, *131*, 195–204.

Ng, K. S., Moo, C. -S., Chen, Y. -P., & Hsieh, Y. -C. (2009). Enhanced coulomb counting method for estimating state-of-charge and state-of-health of lithium-ion batteries. *Applied Energy*, *86*, 1506–1511.

Norian, K. H. (2013). Measuring electrical components of lithium ion battery at different states of charge. *Journal of Power Sources*, *242*, 714–717.

Plett, G. L. (2004). Extended kalman filtering for battery management systems of LiPB-based HEV battery packs. Part 3. State and parameter estimation. *Journal of Power Sources*, *134*, 277–292.

Prasad, G. K., & Rahn, C. D. (2014). Model based identification of aging parameters in lithium ion batteries. *Journal of Power Sources*, *257*, 1–11.

Rahimi-Eichi, H., Baronti, F., & Chow, M. -Y. (2014). Online adaptive parameter identification and state-of-charge coestimation for lithium-polymer battery cells. *IEEE Transactions on Industrial Electronics*, *61*(4), 2053–2061.

Reif, K., Günther, S., Yaz, E., & Unbehauen, R. (1999). Stochastic stability of the discrete-time extended Kalman filter. *IEEE Transactions on Automatic Control*, *44*(4), 714–728.

Sepasi, S., Ghorbani, R., & Liaw, B. Y. (2014). A novel on-board state-of-charge estimation method for aged Li-ion batteries based on model adaptive extended Kalman filter. *Journal of Power Sources*, *245*, 337–344.

Simon, D. (2012). *Optimal state estimation: Kalman, H_∞, and nonlinear approaches*. Hoboken, New Jersey: Wiley-Interscience.

Sun, F., Hu, X., Zou, Y., & Li, S. (2011). Adaptive unscented kalman filtering for state of charge estimation of a lithium-ion battery for electric vehicles. *Energy*, *36*, 3531–3540.

Tie, S. F., & Tan, C. W. (2013). A review of energy sources and energy management system in electric vehicles. *Renewable and Sustainable Energy Reviews*, *20*, 82–102.

USABC (1996). *Electric vehicle battery test procedures manual. Revision 2*.

Waag, W., Käbitz, S., & Sauer, D. U. (2013). Experimental investigation of the lithium-ion battery impedance characteristic at various conditions and aging states and its influence on the application. *Applied Energy*, *102*, 885–897.

Wang, J., Cao, B., Chen, Q., & Wang, F. (2007). Combined state of charge estimator for electric vehicle battery pack. *Control Engineering Practice*, *15*, 1569–1576.

Wang, B., Li, S. E., Peng, H., & Liu, Z. (2015). Fractional-order modeling and parameter identification for lithium-ion. *Journal of Power Sources*, *293*, 151–161.

Xiong, R., He, H., Sun, F., & Zhao, K. (2013). Evaluation on state of charge estimation of batteries with adaptive extended Kalman filter by experiment approach. *IEEE Transactions on Vehicular Technology*, *62*(1), 108–117.

Xiong, R., Sun, F., Gong, X., & He, H. (2013). Adaptive state of charge estimator for lithium-ion cells series battery pack in electric vehicles. *Journal of Power Sources*, *242*, 699–713.

Yan, J., Xu, G., Qian, H., & Xu, Y. (2010). Robust state of charge estimation for hybrid electric vehicles: Framework and algorithms. *Energies*, *3*, 1654–1672.

Yu, Q., Xiong, R., Lin, C., Shen, W., & Deng, J. (2017). Lithium-ion battery parameters and state-of-charge joint estimation based on h-infinity and unscented Kalman filters. *IEEE Transactions on Vehicular Technology*, *66*(10), 8693–8701.

Zhang, Z., Cheng, X., Lu, Z., & Gu, D. (2017). SOC estimation of lithium-ion batteries with AEKF and wavelet transform matrix. *IEEE Transactions on Power Electronics*, *32*(10), 7626–7634.

Zhang, F., Liu, G., Fang, L., & Wang, H. (2012). Estimation of battery state of charge with H_∞ observer: Applied to a robot for inspecting power transmission lines. *IEEE Transactions on Industrial Electronics*, *59*(2), 1086–1095.

Zhao, D., Gao, F., Massonnat, P., Dou, M., & Miraoui, A. (2015). Parameter sensitivity analysis and local temperature distribution effect for a PEMFC system. *IEEE Transactions on Energy Conversion*, *30*(3), 1008–1018.

Zhao, L., Ji, G., & Liu, Z. (2017). Design and experiment of nonlinear observer with adaptive gains for battery state of charge estimation. *Energies*, *10*, 2046.